

Observer-based Control for a Torque Converter Lock-up clutch Utilizing a Steady-state Torque Map

Byungjun Kim, Seibum B. Choi, *Member, IEEE* Youngkwon Kim

Abstract—Torque converter slip control is one of the most important ways to improve vehicle fuel economy and ride comfort without changing hardware. Several model-based feed-forward controllers have been proposed to improve control performance. However, model-based controllers depend on a torque map (lookup table) measured in steady-state; thus, they have errors in transient situations. Therefore, this paper proposes an observer-based feed-forward controller that utilizes a steady-state torque map. To overcome the limitation of the torque map and unknown road torque, a novel observer is proposed that makes it possible to use both the advantages of a torque map and a vehicle driveline model. The proposed observer can adjust dependency on the map in real-time with the observer index. A fuzzy logic-based observer index can obtain near-optimal gain with minimal tuning and low computation. In addition, a real-time torque converter map-update algorithm using a Recursive Least Square (RLS) method is proposed. As a result, the feed-forward controller is designed considering the error of torque maps. The effectiveness of the proposed observer and feed-forward controller were verified using a simulation based on experimental data from an actual vehicle.

Index Terms—Torque converter, Lock-up clutch, Slip control, Observer-based control, Output shaft torque estimation, Model-based control, Recursive least square estimation

I. INTRODUCTION

IN a vehicle with an automatic transmission (AT), the torque converter (TC) amplifies the engine torque and transmits it to the transmission. However, energy loss has occurred because torque converters transmit torque using a fluid. Therefore the mechanical device, a lock-up clutch, is used to transmit the torque and minimizes energy loss. However, these mechanical couplings cannot absorb vibrations from the engine and gear shifting, so they deteriorate ride comfort. To use the advantages of both couplings, aggressive control such as micro slip (~ 10 rpm) control is required to minimize the range of fluid coupling. Therefore, it is essential to improve the performance of the slip controller.

This research was partly supported by the Hyundai Motor Company; the BK21+ program through the NRF funded by the Ministry of Education of Korea; the Technology Innovation Program (20010263, Development of innovative design for UX environment improvement and commercialization model of wheelchair electric motorization kit with enhanced portability and convenience) and (20014983, Development of autonomous chassis platform for a modular vehicle) funded By the Ministry of Trade, Industry & Energy(MOTIE, Korea); the National Research Foundation of Korea(NRF) grant funded by the Korea government(MSIP) (No. 2020R1A2B5B01001531); the Technology Innovation Program.

Byungjun Kim and Seibum B. Choi are with the Department of Mechanical Engineering Korea Advanced Institute of Science and Technology (KAIST), Daejeon, 34141, Korea (email: asx9608@kaist.ac.kr; sbchoi@kaist.ac.kr). Youngkwon Kim is with the Department of IATD Hyundai motor company, Hwaseong, 18280, Korea (email:k2rifle@hyundai.com)

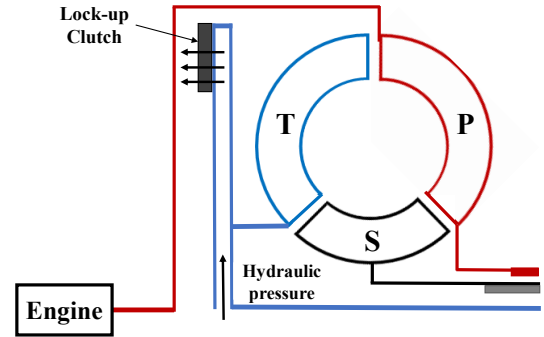


Fig. 1: Torque converter Lock-up clutch system

The TC lock-up clutch system is shown in Fig. 1. The torque converter is composed of a pump (P), a turbine (T), and a stator (S). The engine torque can be transmitted to the transmission connected to the turbine shaft by a torque converter or lock-up clutch. Therefore, by controlling the torque of the lock-up clutch, the input-to-output ratio of the torque transmitted is adjusted to track the target slip.

Because the nonlinearity and uncertainty of the torque converter slip system are severe, most studies have used feedback controllers such as H_∞ control and other robust control methods. Osawa, Hibino and Dourra [1]–[3] applied H_∞ control to a slip-control. Also Hibino [4] use loop shaping method to optimize a sensitivity function. In the case of all robust controls based on error feedback, there is a limitation in performance in the transient region. Also, the control performance decreases as the robustness of the controller increases according to the system uncertainty. Especially in torque converter systems, as the sensor noise of production vehicles is significant, input becomes noisy if the feedback gain is immense. If a simple filter such as a low pass filter is used to solve the noise, phase lag occurs. Then, engagement is not possible at the desired time, which causes a shock due to feedback. Therefore, model-based feed-forward control plays an essential role in overall control performance. Also, if feed-forward is used, the feedback controller can be designed more aggressively by focusing on performance. As a result, model-based feed-forward control is required to reduce system uncertainty and dependence on feedback control.

There have been several approaches to designing a feed-forward controller. Hebbale [5] performed model-based feed-forward control of the torque converter slip system. The study is based on a simple TC model. Therefore, the control performance can be significantly degraded depending on the engine torque error and TC maps. The engine torque map

has a large nonlinearity and describes only the steady-state. Therefore, the accuracy of the engine torque map is high in steady-state, but the difference between the torque map and the actual torque is significant during the transient. Hahn's nonlinear robust control [6] has the advantage of being more robust since it estimates the road torque and output shaft torque. Yoshio [7] applies the nonlinear output regulation to the TC control. It shows high performance, but it depends on the first-order lag torque model and has a disadvantage in that the time-varying coefficient of the model must be known. Gao uses backstepping control [8] for clutch slip control. It has the advantage of the robustness of model uncertainties and unmodelled dynamics. However, they have the same problem when there is an error in torque maps. Oh [9] estimated the uncertainty of the engine torque, but there are excessive parameters to converge at once. Diachuk [10] proposes precise models and a method for coordinating the engine control and operating model, but too many parameters have to be known.

The pump torque and turbine torque of TC can be obtained from an empirical map, or a dynamic model [11]–[13]. The model requires fitting through experimental data, and the parameters may vary for each torque converter. Lee [14] proposes control-oriented dynamic model for torque converter. The proposed model can describe the dynamic well that differs from the existing static map by using hydrodynamics. However, it may vary depending on the shape of the torque converter, and it is not easy to obtain coefficients. Yi [15] suggested nonlinear observers estimate turbine torque, but there were still excessive tuning parameters. Therefore, the engine, pump, and turbine torque obtained from the map may differ from the actual torques, and this condition should be considered for control. Hahn et al. [6] proposed a robust controller by estimating turbine torque and load torque, and Han [16] proposed a fuzzy logic controller. Since a neural network or fuzzy logic was used to estimate the turbine torque, extensive data about the vehicle powertrain must be provided. In addition, the control accuracy depends entirely on the accuracy of the engine map. Mishra [17] proposes on-line identification method of a torque converter model. It has the advantage of being able to obtain the turbine torque in real-time accurately, but it is not clear whether the persistence of excitation can be guaranteed in actual vehicle driving and whether it is robust to sensor noise.

There have been many studies to estimate the output shaft torque. However, most studies have fully trusted the steady-state engine torque map or do not use a torque map at all [18]–[23]. If a torque map is not used, the advantage of an accurate torque map in steady-state vanishes. Many studies use optimal observer gain with the Riccati equation (e.g., extended Kalman filter), which requires large computations [24]–[26]. It is a fatal flaw in production vehicle applications. In addition, the advantages of a torque map and a driveline model cannot be combined because the optimal gain of the Kalman filter is obtained by solving a stochastic problem without considering the system's current state.

To this end, this paper proposes an observer-based feed-forward controller for torque converter slip control. In summary, there are three developments; 1) An observer that can ad-

just the dependency of each measurement considering current states is proposed and an observer gain that satisfies stability can be obtained. The observer has the same tuning parameters and amount of computation as the Luenberger observer but it performs better than the Kalman filter in the TC slip system. 2) Combine the proposed observer and disturbance-decoupled observer (DDO), take advantage of both observers, and reduce the sensitivity to sensor noise in DDO [27]. 3) Using output shaft torque by the proposed observer and corrected TC torque map by RLSE, a model-based feed-forward controller is constructed.

In the remainder of this paper, Section II presents a dynamic model of the TC slip system and the TC map calibration process. Also, an observer-based feed-forward controller is described as well. In Section III the observer design is described, while in section IV, the experimental data-based simulation configuration is described. Finally, the performance of the proposed algorithm, as indicated by the simulation results, is presented in section V.

II. SYSTEM MODELING AND FEED-FORWARD CONTROLLER

A. System Modeling

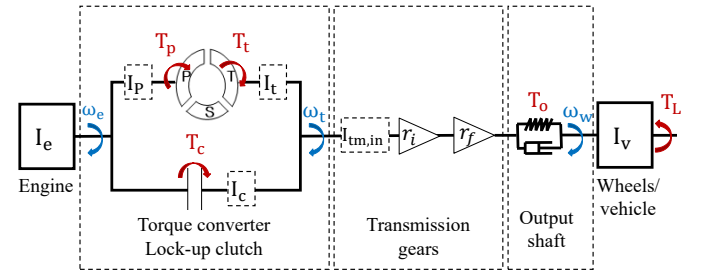


Fig. 2: Lumped inertia driveline model of AT vehicle

$$(I_e + I_p)\dot{\omega}_e = T_e - T_c - T_p \quad (1a)$$

$$(I_t + I_c + I_{tm.in})\dot{\omega}_t = T_t + T_c - \frac{T_o}{r_i r_f} - T_{drag} \quad (1b)$$

$$(I_{wt} + I_{veh})\dot{\omega}_w = T_o - T_L \quad (1c)$$

$$T_o = k_{eq} \left(\frac{1}{r_i r_f} \theta_t - \theta_w \right) \quad (1d)$$

Oh, and Kim [28], [29] propose a lumped inertia driveline model of a DCT (Dual clutch transmission) vehicle. The proposed model was applied to AT vehicle, and Fig. 2 shows a lumped inertia driveline model of an AT vehicle with a TC. In detail, spring and damper models can be applied between the lock-up clutch and the turbine or to the input shaft, but it is very stiff compared to the output shaft. The compliance model of the driveline can be modeled using a single equivalence spring in the output shaft. Thus, output shaft torque can be expressed by multiplying angle difference and equivalence spring stiffness (k_{eq}). The torque balance equation of the lumped inertia driveline model can be expressed as (1).

Where I, ω, θ, T , and r indicate rotational inertia, angular velocity, angle, torque, and gear ratio. The subscripts

$e, p, t, c, o, L, tm.in, i, f, b$ and v mean engine, pump, turbine, clutch, output shaft, road load, transmission input shaft, initial gear, final gear and vehicle. In equation (1), the sum of I_e and I_p is set to I_1 . The expression, $I_t + I_c + I_{tm.in}$ is set to I_2 , and $I_{wt} + I_{veh}$ is set to I_3 . T_{drag} represents the drag torque which is the torque lost due to transmission inefficiency. T_L , the road torque, means the load on the vehicle due to external conditions, such as the weight, slope of the road, and rolling resistance, and is expressed by (2). $r_w, m_v, \theta_r, K_{rr}, \rho, v_x, C_d$, and A mean wheel radius, vehicle mass, road gradient angle, rolling resistance, air density, vehicle velocity, aerodynamic drag coefficient, and vehicle front area. However, it is not an accurate model, so it can only obtain approximate values. The road torque does not change rapidly, but it is difficult to know and measure in production vehicles, and it changes over time. The terms ω_e, ω_t , and ω_w are angular velocities that can be measured in production vehicles.

$$T_L = r_w(m_v g \sin(\theta_r) + K_{rr} m_v g \cos(\theta_r)) + \frac{1}{2} \rho v_x^2 C_d A \quad (2)$$

In (1a), T_e can be obtained in real-time using the engine torque map. Because the torque map is measured in steady-state, an error occurs between the actual torque and the map in the transient region. In (1a), (1b), T_p and T_c can be obtained from the TC map. The error of the map is not large due to its small nonlinearity compared to the engine, but the torque may be different even with the same TC. Therefore, even if the same engine and TC are used, the torque generated under the same conditions may be different for each vehicle, so it must be considered.

B. Feed-forward Controller

When using a model for feed-forward control, $T_{c,d}$ for control can be obtained through (1a) as shown in (3a). It is simple and accurate in the steady-state, but performance is poor in the transient region due to issues with the torque map.

$$T_{c,d} = T_e - T_p - I_1 \dot{\omega}_e \quad (3a)$$

$$T_{c,d} = -T_t + \frac{T_o}{r_i r_f} + T_{drag} + I_2 \dot{\omega}_t \quad (3b)$$

When using the driveline model as (1b), the term $T_{c,d}$ can be obtained through another method, such as indicated in (3b). This method uses only the turbine torque, so engine torque is not required. However, it is difficult to know T_o and T_{drag} . The advantages of the two methods can be combined through the observer proposed in the next chapter. The TC map can also be updated in real-time. The overall feed-forward algorithm using the torque estimation and map update can be represented as shown in Fig. 3

C. Torque converter map calibration

The $T_{c,d}$ calculated using (3b) is not related to the engine torque map, but it is affected by the TC map error. Therefore, the TC map should be updated in real-time to reduce errors.

Fig. 4 shows the TC map with the torque ratio, $t(\lambda) = T_t/T_p$, and capacity factor, $C(\lambda) = \omega_p/\sqrt{T_p}$, which are

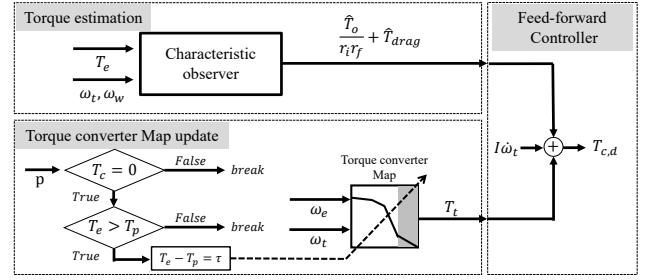


Fig. 3: Schematic of feed-forward controller

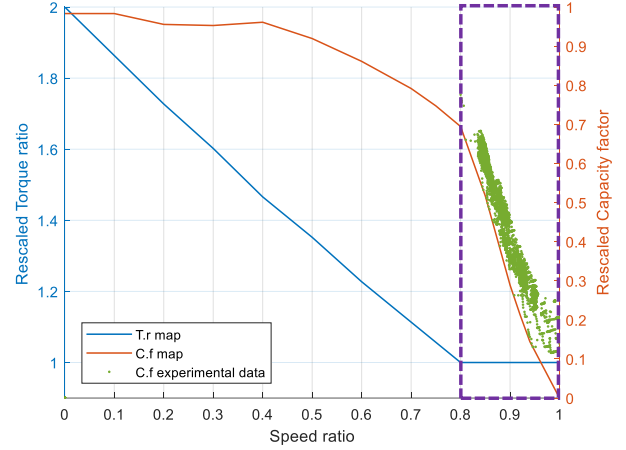


Fig. 4: Torque converter map with experimental data

function of speed ratio, $(\lambda) = \omega_t/\omega_p$. For reasons of confidentiality, the torque ratio and capacity factor were scaled to 1-2 and 0-1, respectively. The lock-up clutch usually operates between a 0.8 and 1 speed ratio. Therefore, in Fig. 4, the region of the slope of the capacity factor when the x-axis is between 0.8 and 1 is the most important. This slope is obtained in real-time when the engine torque and the pump torque are equal. When the control pressure is less than the pressure corresponding to the torque kissing point, which is the point that torque starts to be transmitted, the clutch torque is always zero. In this region, T_e and T_p should be equal, but there is a difference when calculated using a map. Therefore, the slope can be obtained in real-time using this difference. The slope is not perfectly linear when the speed ratio is between 0.8 and 1. However, as can be seen from the experimental results in Fig. 4, due to noise in the measurement of the speed ratio and disturbance, a precise nonlinear model is not required in the corresponding region. Therefore, it will be helpful, even if only the first approximated slope is found. The slope is updated in real-time using the Recursive Least Square estimation (RLSE) method as shown in (4) [30]. y_k means k step's measurement, and x_k is the state that should be estimated. In this case, x_k represents the slope. Also, it has a relationship of $y_k = h_k x_k$, and h_k can be obtained from the sensor with eq.(4). K_k is the estimator gain matrix, and P_k is the estimation-error covariance matrix that they are automatically computed in every time step. λ is a forgetting factor that can give less weight to older errors, and it is a

tuning parameter. The slope is easily obtained using the fact that the capacity factor curve passes through (1,0) and assumes that the capacity factor to speed ratio is linear between 0.8 and 1 speed ratio. Measurement y is a virtual sensor constructed using the engine torque map and the angular velocity sensor. Despite using the engine torque map, the error of the map is not large when the speed ratio is between 0.8 and 1 because the engine is in a steady state. The initial gradient is set to the gradient of the existing map, and as the data gradually increases, it converges within the range, including the actual value. The converging bound is proportional to how nonlinear the actual slope is and the magnitude of the sensor noise. As a result, it is possible to design a feed-forward controller in consideration of the errors occurring in both the engine map and the TC map.

$$\begin{aligned} y_k &= T_{e,k} - (I_e + I_p)\dot{\omega}_e \\ H_k &= \frac{\omega_{t,k}}{\omega_{e,k}} - 1 \\ K_k &= P_{k-1}H_k^T(H_kP_{k-1}H_k^T + \lambda)^{-1} \\ \hat{x}_k &= \hat{x}_{k-1} + K_k(y_k - H_k\hat{x}_{k-1}) \\ P_k &= \frac{1}{\lambda}(I - K_kH_k)P_{k-1} \end{aligned} \quad (4)$$

III. OBSERVER DESIGN

The observer proposed in this paper can change the observer gain according to the characteristics of the plant (clutch slip system) state. When applying the proposed observer to the TC slip system, observer relies on the torque map to improve the convergence in the steady-state and reduce the dependence of the torque map in the transient. Therefore, the observer needs an observer index to determine whether the current plant is in a steady state or a transient.

In torque estimation, it is impossible to estimate T_o and T_{drag} independently due to an observability issue. However for $T_{c,d}$, only the sum of the two torques needs to be estimated, so the observer's state is configured as $[\omega_t, \frac{T_o}{r_i r_f} + T_{drag}]'$. The sum of the torques can be estimated through the DDO configured below as (5) and, (6). This method has the advantage of reducing the number of states by replacing unmodeled dynamics with a sensor, but it causes a problem that is sensitive to sensor noise [31].

$$\begin{aligned} I_2\dot{\omega}_t &= T_t + T_{c,m} - \frac{T_o}{r_i r_f} - T_{drag} \\ \frac{\dot{T}_o}{r_i r_f} + \dot{T}_{drag} &= \frac{k_s}{r_i r_f} \left(\frac{1}{r_i r_f} \omega_t - \omega_w \right) \end{aligned} \quad (5)$$

$$\dot{\hat{x}}(t) = Ax(t) + A_d(t) + Bu(t) + L_k(t)(Y(t) - C\hat{x}(t)) \quad (6)$$

where $x = [\omega_t \quad \frac{T_o}{r_i r_f} + T_{drag}]'$, $u = T_{c,m}$ and

$$\begin{aligned} A &= \begin{bmatrix} 0 & -\frac{1}{I_2} \\ \frac{k_s}{(r_i r_f)^2} & 0 \end{bmatrix}, A_d = \begin{bmatrix} \frac{T_t}{I_2} \\ -\frac{k_s}{r_i r_f} \omega_w \end{bmatrix}, \\ B &= \begin{bmatrix} -1 \\ 0 \end{bmatrix}, C = \begin{bmatrix} 1 & 0 \\ 0 & 1 \end{bmatrix} \end{aligned}$$

Because the transmission efficient (T_{drag}) changes slowly, the observer can be constructed by setting the derivative of T_{drag} as zero. Using a DDO, a part of the model and unknown input can be replaced with a wheel angular velocity sensor. As a result, because (1c) is not used, it is possible to estimate the states without knowing road torque. Therefore, it is possible to reduce the error of the existing estimation method, which is caused by assuming that the road torque is constant. However, this method is sensitive to sensor noise because it replaces the model with a sensor value. From (6), as the gear ratio (r_i, r_f) decreases, the wheel speed sensor noise is amplified where the second term of the A_d matrix. However, this is not a problem with the proposed observer. When the gear ratio is low, the vehicle speed is the fast and mostly steady-state situation. Therefore, the effect of the noise can be reduced by increasing dependence on the engine torque map to the observer.

Measurement Y , as used in the observer, includes $y_1 = \omega_t$ and virtual sensor, $y_2 = \frac{T_o}{r_i r_f} + T_{drag}$. The term y_2 can be obtained by adding (1a) and (1b). As can be seen in Fig. 4, the torque ratio is 1 because the slip ratio is 0.8-1 in the control area of the TC. Therefore, $T_t = T_p$, and a virtual sensor can be obtained as shown in (7). Because the torque map is accurate and $\dot{\omega}_e, \dot{\omega}_t$ can be approximated to zero in steady-state, the virtual sensor is accurate in steady-state. T_c, T_p , and T_t are not required for calculating the virtual sensor. Therefore, there is no need to consider error in the clutch torque model and TC map.

$$y_2 = \frac{T_o}{r_i r_f} + T_{drag} = T_e - I_1\dot{\omega}_e - I_2\dot{\omega}_t \approx T_e \quad (7)$$

A. Stability Analysis

Observer gain L_k in the proposed observer is a two-by-two matrix, and there are four tuning parameters. When using a Kalman filter, the optimal gain can be obtained in real-time, but there is the disadvantage of a tremendous amount of calculation [30]. Therefore, the near-optimal gain is obtained using the initial tuning parameters and open-loop observer index. The initial tuning parameter L_1 and L_2 are set to a stable gain when using a single sensor and a virtual sensor, respectively. It can be determined by making \bar{A}_1 and \bar{A}_2 Hurwitz in (8).

$$\begin{aligned} e_{1,k+1} &= (A - L_1C_1) = \bar{A}_1 e_{1,k} \\ e_{2,k+1} &= (A - L_2C_2) = \bar{A}_2 e_{2,k} \end{aligned} \quad (8)$$

where,

$$C_1 = \begin{bmatrix} 1 & 0 \end{bmatrix}, C_2 = \begin{bmatrix} 0 & 1 \end{bmatrix}, L_1 = \begin{bmatrix} L_{11} \\ L_{21} \end{bmatrix}, L_2 = \begin{bmatrix} L_{12} \\ L_{22} \end{bmatrix}$$

In order for \bar{A}_1, \bar{A}_2 to always be Hurwitz, all eigenvalues of \bar{A}_1, \bar{A}_2 must be negative and through this, the observer gain must satisfy (9).

$$\begin{aligned} L_{11} &> 0, \quad L_{21} < \frac{k}{(r_i r_f)^2} \\ L_{22} &> 0, \quad L_{12} > -\frac{1}{I_2} \end{aligned} \quad (9)$$

If (8) satisfies, the error dynamics (10) is asymptotic stable.

$$e_{k+1} = (A - L_k C) = \bar{A} e_{1,k} \quad (10)$$

where, $0 \leq \alpha \leq 1$ and

$$L_k = [(1 - \alpha)L_1 \quad \alpha L_2] = \begin{bmatrix} (1 - \alpha)L_{11} & \alpha L_{12} \\ (1 - \alpha)L_{21} & \alpha L_{22} \end{bmatrix}$$

To make all eigenvalues of \bar{A} negative, (11) should be satisfied. However, because of the condition $0 \leq \alpha \leq 1$, (9), and condition (11) are always satisfied. Therefore, adjusting the α is the same as pole placement in the stable region.

$$\left(\frac{1}{I_2} + \alpha L_{12}\right) \left(-\frac{k}{(r_i r_f)^2} + (1 - \alpha)L_{21}\right) < 0 \quad (11)$$

Through L_1 , L_2 , and observer index(α), the observer gain that satisfies stability is calculated in real-time. To ensure that the observer is always stable regardless of the size of A and C, a linear matrix inequality (LMI) based condition is as follows [32]:

Theorem 1 : For the error dynamics of an observer with variable gain $0 \leq \alpha \leq 1$, the system described by (6) is asymptotically stable if there exist positive definite matrices P_1 and P_2 satisfying

$$P_1 > 0, (A - L_1 C_1)^T P_1 + P_1 (A - L_1 C_1) < 0 \quad (12a)$$

$$P_2 > 0, (A - L_2 C_2)^T P_2 + P_2 (A - L_2 C_2) < 0 \quad (12b)$$

with

$$(L_1 C_1 - L_2 C_2)^T (P_1 - P_2) + (P_1 - P_2) (L_1 C_1 - L_2 C_2) \geq 0 \quad (13)$$

Proof : The summation of $\alpha \times (12a)$ and $(1 - \alpha) \times (12b)$:

$$\begin{aligned} & A^T (\alpha P_1 + (1 - \alpha) P_2) + (\alpha P_1 + (1 - \alpha) P_2) A \\ & - \alpha (C_1^T L_1^T P_1 + P_1 L_1 C_1) \\ & - (1 - \alpha) (C_2^T L_2^T P_2 + P_2 L_2 C_2) < 0 \quad (14) \end{aligned}$$

For simplicity, denote

$$P^* := \alpha P_1 + (1 - \alpha) P_2 \quad (15)$$

By multiplying $(\alpha + 1 - \alpha)$ to (14)

$$\begin{aligned} & A^T P^* + P^* A - \alpha^2 (C_1^T L_1^T P_1 + P_1 L_1 C_1) \\ & - \alpha (1 - \alpha) (C_1^T L_1^T P_1 + P_1 L_1 C_1) \\ & - \alpha (1 - \alpha) (C_2^T L_2^T P_2 + P_2 L_2 C_2) \\ & - (1 - \alpha)^2 (C_2^T L_2^T P_2 + P_2 L_2 C_2) < 0 \quad (16) \end{aligned}$$

Since L_k is composed with L_1, L_2 and, α , It can be expressed as (17).

$$\alpha L_1 C_1 + (1 - \alpha) L_2 C_2 = L_k C \quad (17)$$

If we add and subtract $\alpha(1 - \alpha)(C_1^T L_1^T P_2 + P_2 L_1 C_1) + \alpha(1 - \alpha)(C_2^T L_2^T P_1 + P_1 L_2 C_2)$ to left side of (14) so that the equation does not change, we can rearrange (16) with (17). With simple calculation then using $\alpha(1 - \alpha) > 0$ and (13), Inequality becomes:

$$(A - L_k C)^T P^* + P^* (A - L_k C) < 0 \quad (Q.E.D.) \quad (18)$$

Because $P^* > 0$, there is always a P^* that satisfies the Lyapunov inequality (18).

Consider the typical P case; in this case, the stability conditions of Theorem 1 can be simplified as follows.

Corollary 1 : Assume that $P_1 = P_2 = P$. The system described by (6) is asymptotically stable if there exists a positive definite matrix P satisfying

$$\begin{aligned} & P > 0, (A - L_1 C_1)^T P + P (A - L_1 C_1) < 0 \\ & (A - L_2 C_2)^T P + P (A - L_2 C_2) < 0 \quad (19) \end{aligned}$$

In most systems, P that satisfies $P_1 = P_2$ can be found. Therefore, if the initial tuning parameters L_1 and L_2 are well set, the observer can always satisfy the stability regardless of the time-varying observer index. In the TC slip system, the P value that satisfies (19) can be obtained, so by setting L_1 and L_2 that satisfy (9), an asymptotically stable observer can be constructed regardless of α . Therefore, it can also be proved by the Hurwitz method with (8)-(11). In conclusion, using the observer index, the observer pole is moved to the desired position within the left half-plane, and the dependence of each sensor is adjusted in real-time.

B. Observer index

The observer index (α) is an index indicating how transient the situation is and has a value between 0 and 1. Therefore, the closer to 1 means the less dependence on the engine torque map. If the observer index has a value of 0 or 1, either L_1 or L_2 in Equation (8) becomes 0. It means that only one sensor is used, and it does not affect the stability of the observer according to the existing L_1 and L_2 stability conditions. The observer index can be obtained using fuzzy logic as proposed by Cheli [33]. The configuration of the observer index is shown in Fig. 5. The states used in the fuzzy logic are the observer states x_1 and x_2 , and the engine index (τ) that can preview the trend of the engine torque. Engine index (τ) has the same configuration as the observer index. The states of the engine index fuzzy logic are engine torque (T_e) and acceleration position sensor (APS); therefore, the engine index indicates how transient the engine condition is. The weights are tuned according to how well the states represent "how transient." The sum of the weights should be 1, and almost the same weight is given to the three states. Since the turbine speed corresponds to the vehicle's output, the weight for the engine index and engine map is slightly higher than that of the turbine speed.

IV. SIMULATION AND EXPERIMENTAL CONFIGURATION

A simulation based on experimental data was constructed to verify the proposed algorithm. In the experiments, many values are difficult to measure, such as transmission efficiency and output shaft torque, due to sensor attachment problems. Therefore, to obtain values that are difficult to measure in the vehicle, a simulation was configured, and the vehicle velocity

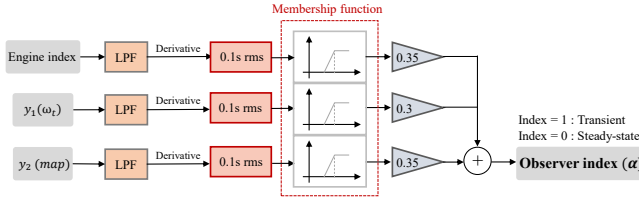


Fig. 5: Configuration of the observer index

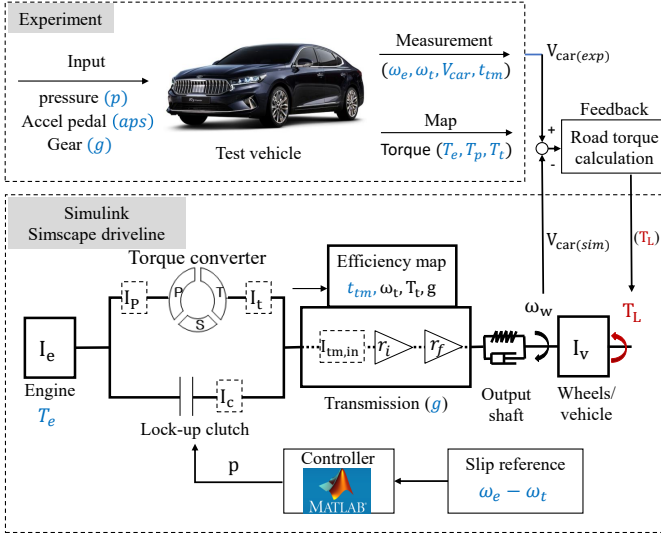


Fig. 6: Experimental data based simulation Configuration

was feedback using the experimental data to increase the reliability of the data. When the load torque was calculated to provide feedback, a low pass filter was used to assure that change was not too rapid. White noise equal to the noise level of production vehicle sensors was added to the simulation sensor. Also unlike (1d), the actual damping coefficient was used without ignoring the damping for simulation. The vehicle used in the experiment, and the simulation configuration, are shown in Fig. 6.

In production vehicles, ω_e , ω_t , and transmission oil temperature (t_{tm}) can be measured. T_e , T_p , and T_t can be obtained in real-time using the torque map. The simulation uses experimental data such as T_e , aps , p , g , and t_{tm} as inputs. The transmission efficiency is obtained through a four-dimensional map consisting of input shaft torque, input shaft angular velocity, transmission oil temperature, and gear ratio. The map was constructed through a single-piece experiment. As a result, a simulation that fits well with the experimental results was constructed. Experiments were conducted for two typical situations as shown in Fig. 7, and Fig. 8. V_{car} is calculated from simulation, using driveline model (1) and torque input from experiment data. Then load torque of the simulation was calculated inversely to match the speed of the simulation and the test vehicle equally. To verify the simulation accuracy, compare the experimental results with the open-loop simulation without a control reference using the same inputs (T_e , T_c , p , aps , g) and vehicle parameters.

In the first case, an engine angular velocity of 1200rpm was maintained, and the clutch pressure was controlled to change

the slip. As shown in Fig. 7a, Case 1 is in a steady state in which the engine torque is almost constant. Because it is in a steady state, the torque obtained from the map and the actual torque is almost the same. In addition, because the torque ratio is close to 1 in the control area, it can be seen that the pump and turbine torque are almost the same. In Fig. 7d, the road torque calculated through the feedback is compared to the road torque model (2). It can be seen that the value obtained through the load torque model and the value of the load torque calculated through the speed feedback are similar.

The second case was a shift from 2nd to 3rd gear through acceleration. Contrary to Case 1, it is a transient situation. Therefore, there may be an error in the actual engine torque and the torque map. In the simulation, (20) is used to implement the actual engine torque. Therefore, in the most transient situation, there is a 15% difference between the actual engine torque (T_e) and the torque map ($T_{e,m}$) with engine index (τ). From Fig. 7, the simulated and experimental results are almost the same when the simulation control input pressure is the same as in the experiment.

$$T_e = T_{e,m} \cdot (1 + 0.15 \cdot \tau \cdot \text{sgn}(\dot{T}_{e,m})) \quad (20)$$

Fig. 11 and Fig. 12 show the simulation results for the same situation as Fig. 7 and Fig. 8. In the simulation, the slip reference is designated by removing noise from the experimental slip data. The sensors used for the observer and control contain noise equal to the actual sensors used in the experiments.

A. clutch torque model

The clutch torque model has been studied for a long time [34]–[36]. Because the lock-up clutch in TC is wet, the wet-clutch torque model must be used. For simulation and control, the wet-clutch torque model consists of the contact friction torque (T_f) and viscous friction torque (T_v), as proposed by Deur [34], and the model was used as shown in (21).

$$\begin{aligned} T_c = T_f + T_v &= N_f \theta_0 \frac{b^3 - a^3}{3} \mu(\omega) p_c \text{sgn}(\omega) \\ &+ N_f \theta_0 \frac{b^4 - a^4}{4} \eta \omega \frac{\phi_f - \phi_{fs}}{h} \\ \mu(\omega) &= \mu_c + (\mu_s - \mu_c) e^{-|\omega/\omega_s|^\delta} + \beta_v |\omega| \end{aligned} \quad (21)$$

Where μ_c and μ_s are the friction coefficient and static friction coefficient, and β_v is the viscous friction coefficient. The term N_f indicates the number of clutches. Then, h is film thickness, a and b are inner and outer radius of the clutch, ϕ_f and ϕ_{fs} are flow factors, η is the fluid viscosity, and ω_s and β_v are Stribeck coefficients. The clutch parameters and coefficients in the simulation are the same as used in the experiment. The other parameters are fitted with the experimental data. However, for reasons of confidentiality, the parameters and fitted data are not shown in this paper.

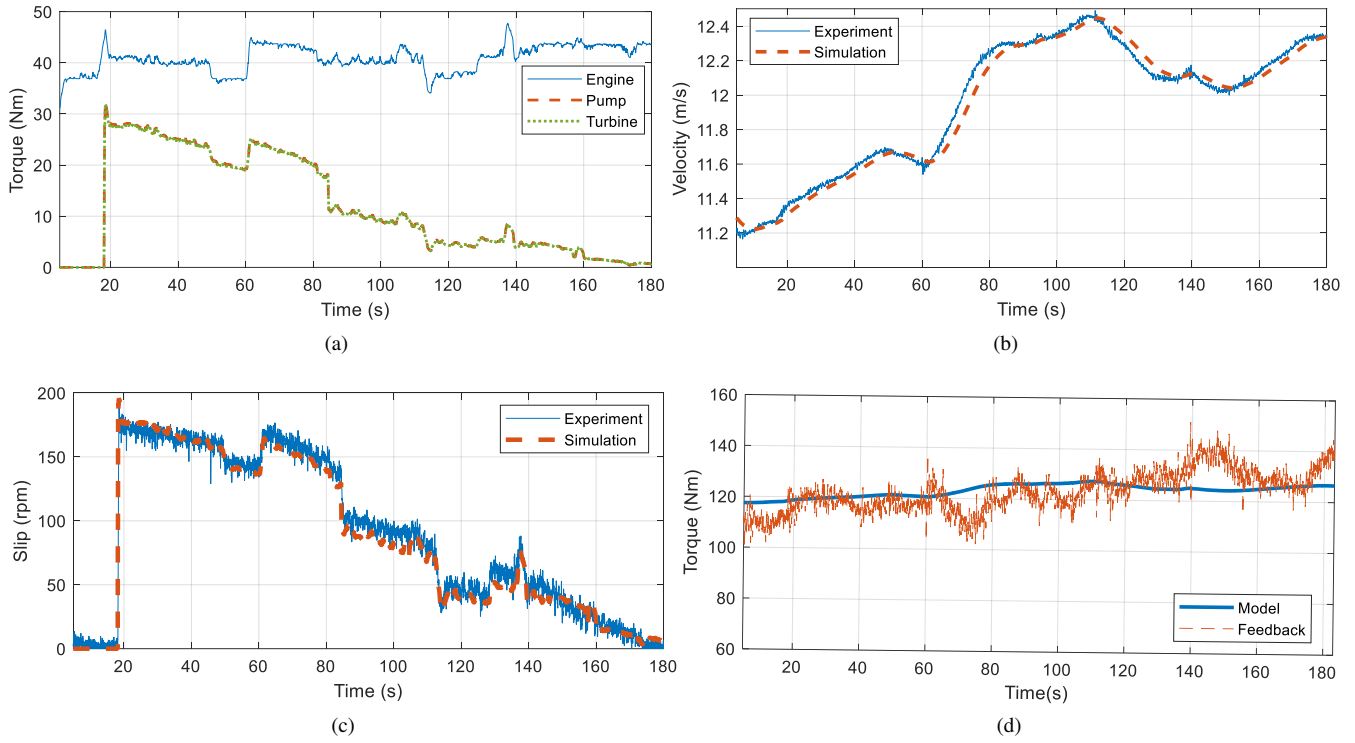


Fig. 7: Experiment and simulation comparison for case 1. (a) Torque. (b) Vehicle velocity. (c) Clutch slip. (d) Road torque.

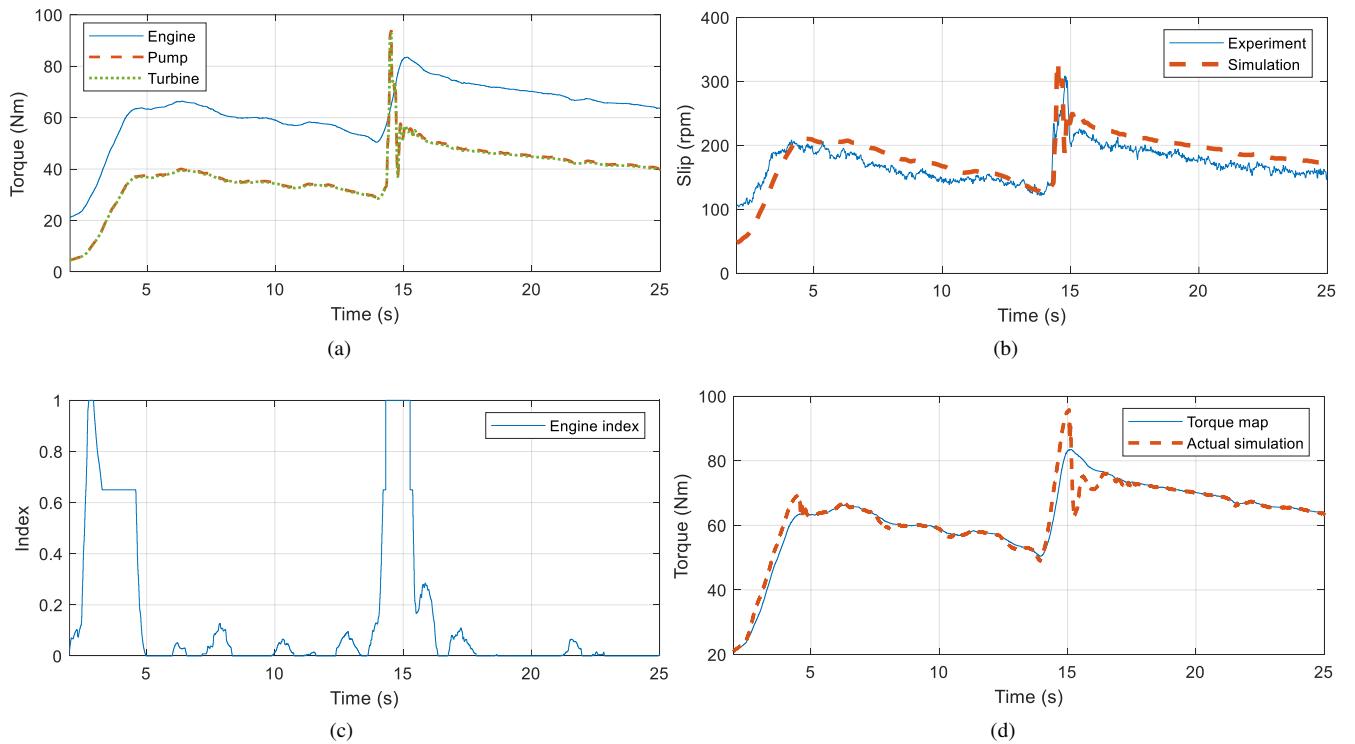


Fig. 8: Experiment and simulation comparison for case 2. (a) Torque. (b) clutch slip. (c) Engine index. (d) Actual engine torque.

V. RESULTS

A. Torque converter map calibration

The map calibration performance of the TC is verified through data-based simulation because the simulation can

obtain the actual torque and TC map. In the simulation, the clutch pressure does not reach the torque kissing condition, thereby allowing it to converge quickly. Fig. 10a is the result

of estimating the slope over time. The initial gradient was set to -2.8 . It can be seen that in the section with a flat slope, the update does not proceed because the update condition is not satisfied or the speed ratio is not between 0.8 and 1 . Fig. 10b shows the accuracy of the map according to the estimated slope. As time goes on, the slope approaches -3.3 and has a slope similar to that on the actual map. Since the map is not perfectly linear, it converges within the range, including the actual value.

Fig. 9 shows the results of the open experiment and the city driving experiment. In the vehicle experiment, the actual value of the slope was not accurately known, and the results were compared through maps measured under steady-state conditions. The open experiment is where the torque converter control is not performed, and $T_c = 0$ is maintained. As can be seen in Fig. 3, the update performs only when $T_c = 0$ and $T_e > T_p$. Therefore, the update of the map is carried out in all sections. A city experiment is data-driven in an actual city where various situations such as launch, stop, cruise, and acceleration occur. Therefore, the map cannot be updated in all sections, and the map can be updated only when the update conditions are satisfied. Compared with the open experimental results, city driving includes several driving situations. Therefore, there are relatively much data near the boundary of the update condition, which causes more sporadic and noisy results than the open experimental result. Therefore, by setting the forgetting factor (λ) close to 1 , the slope converges slowly. The city driving data, which has many launch situations, has many data in the section with a low speed ratio (0.8 - 0.85). However, it can be seen that the average slope is similar to that in the open experiment. The open experiment was conducted for 173 s, and the city driving experiment was conducted for 229 s. The data in Fig 9 shows points only for met update condition. It can be seen that, although the city driving experiment was conducted for much longer, few sections satisfied the update condition. Therefore, there was much less data, and the estimated speed is slower than that in the simulation; however, it does gradually converge

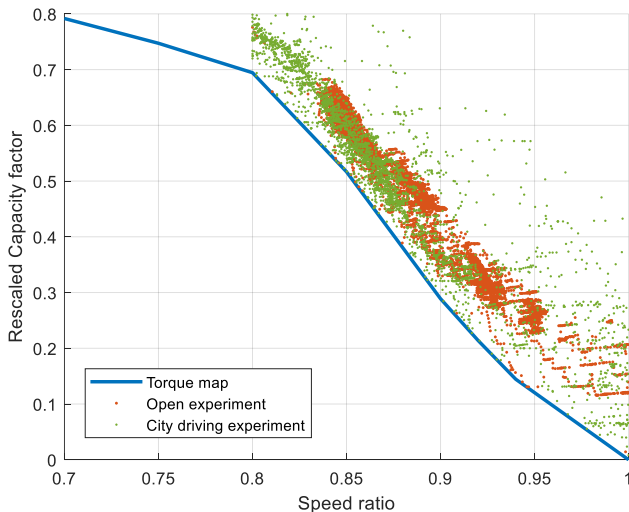
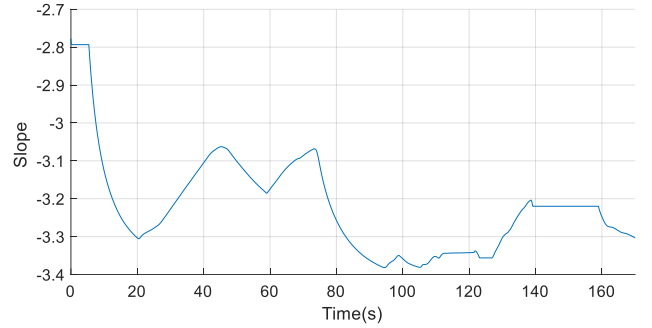
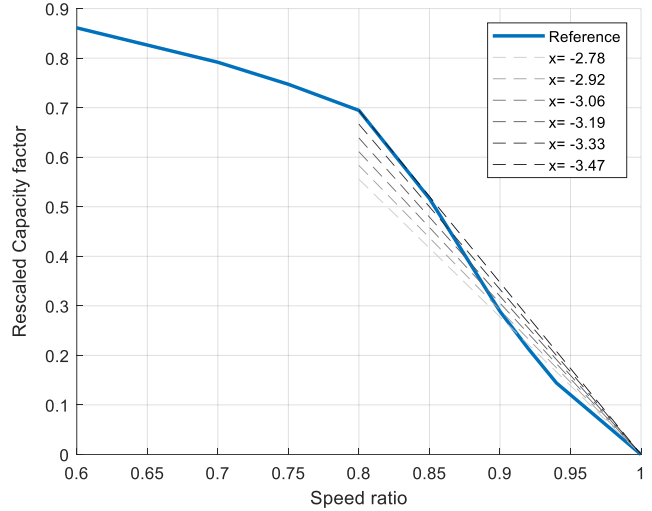


Fig. 9: Map calibration experiment results



(a)



(b)

Fig. 10: Map calibration simulation result. (a) RLSE result. (b) Comparing with actual torque map.

to the actual value over time. It means that the proposed update method is sufficiently effective in general driving situations. Moreover, by setting the initial slope as in the map, better performance can be guaranteed than when the slope is not estimated.

B. Estimation and control result for Case 1

Fig. 11 shows the simulation of the estimation and control results based on the experimental data when 1200 rpm was maintained in 6^{th} gear, as introduced above. The simulation is a steady-state situation with a low observer index, except around 20 and 85 s when the control pressure suddenly changes.

To compare the performance of the observer, we compared the estimator using the fixed gain DDO without using the virtual sensor, the virtual sensor without using the observer, and the proposed observer. For DDO without a virtual sensor, the result is noisy in high gear due to the characteristics of the DDO. For the virtual sensor, it can be seen that the data did not follow the transient part in the enlarged figure of Fig. 11c. As a result of the proposed observer, the result shown is similar to the DDO without a virtual sensor regarding the high observer index and shows a result similar to the virtual sensor in the low observer index. Therefore, it can be seen that the noise

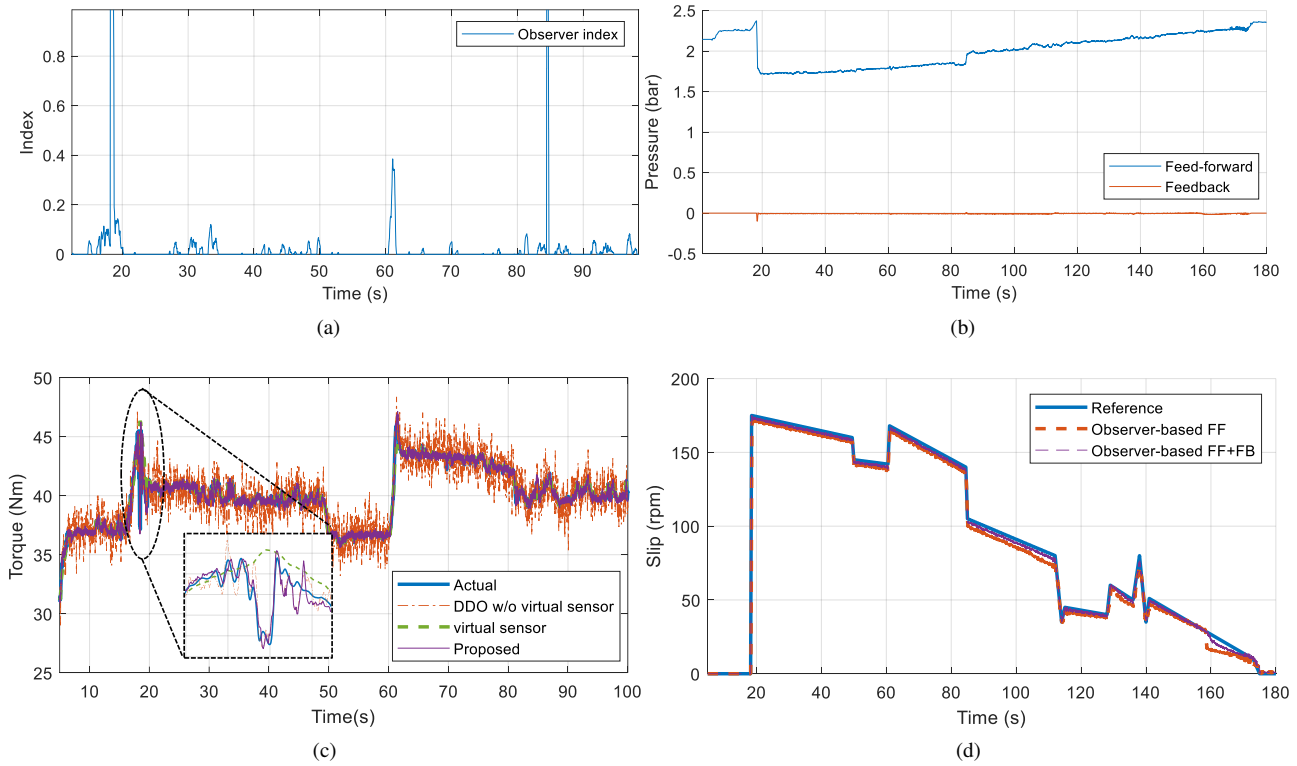


Fig. 11: Case 1: Simulation Result. (a) Observer index. (b) Control input comparison. (c) $\frac{T_o}{r_i r_f} + T_{drag}$ estimation result. (d) Control result.

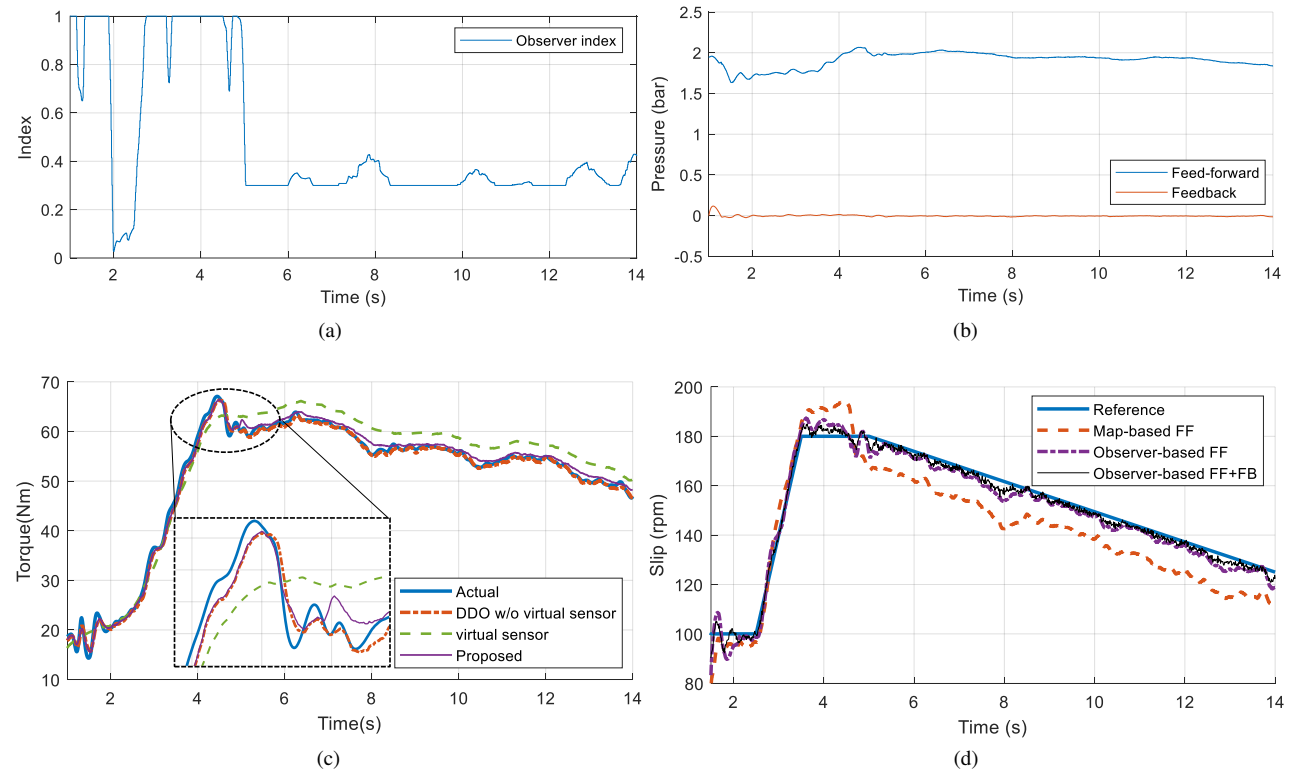


Fig. 12: Case 2: Simulation Result. (a) Observer index. (b) Control input comparison. (c) $\frac{T_o}{r_i r_f} + T_{drag}$ estimation result. (d) Control result.

is reduced in the steady-state situation, and the estimation result converges well and follows the fast dynamics well in the transient situation. In the steady-state, convergence is increased by increasing the dependence on the map. In the transient state, the dependence on the map is reduced. By setting the initial parameters $L_1 = [19 \ 368.13]^T$, $L_2 = [-6.9 \ 100]^T$, it is possible to obtain a near-optimal gain without calculating in real-time, and it shows good convergence. The terms L_1 and L_2 were calculated using the pole placement technique with $(-10, -9)$ for L_1 and $(-0.1, -30)$ for L_2 .

Because this is a steady-state situation, the torque from the engine map and the actual torque is the same. Therefore, for control, there is no significant difference between control using the map and control based on the observer. Fig. 11d shows a result with observer-based feed-forward control and feed-forward with simple PID feedback control. For control results, it shows good performance except for the low slip region, where the nonlinearity and uncertainty of the clutch torque model are considerable. Moreover, in the low-slip region, because the SNR is small, the accuracy of model-based control is not accurate due to the noise effect. As shown in Fig. 11b, it can be confirmed that slip control can be accurately performed, even if the feedback is minimal, due to the high accuracy of the feed-forward controller. In the simulation, the feedback controller is configured using a simple PID controller, however it shows high performance.

C. Estimation and control result for case 2

Case 1 is a highway scenario, so the vehicle has a high and constant speed. In Case 2, the rate of engine torque and output shaft torque is ample because it is an accelerating scenario. Therefore, in case 1, it is a steady situation, but in case 2, it can be said that it is a transient situation.

Fig. 12 shows the simulation results based on the experimental data when accelerated in 2^{nd} gear. It can be seen that the observer index is high compared to Case 1. As can be seen in Fig. 8a, there is a difference between the actual engine torque and the torque through the map. Since it was measured in a steady state, it is not accurate if used in a transient situation (Case 2).

Due to map error, when estimating $\frac{T_o}{r_i r_f} + T_{drag}$, it can be seen that the virtual sensor value obtained from the map is smaller than the actual value around 5 s and that it has an offset error after that. Because the gear is low, it can be seen that the DDO without using a virtual sensor is not sensitive to noise and performs well in the estimation. The proposed observer shows results close to those of the DDO because the observer index is high. The position of the pole is the same as in case 1, but the gear ratio is different. Therefore, the pole placement technique should be used to set $L_1 = [39 \ 366.3]^T$, $L_2 = [-6.9 \ 100]^T$.

Unlike for Case 1, the error between the map and the actual torque is significant, so the model(map)-based feed-forward controller [5] and the proposed observer-based feed-forward controller are compared in Fig. 12d. In the model-based controller, slip error occurs around 5 s because of the torque difference, and it can be seen that there is an offset

error after 5 s. The proposed observer-based control reduces the error. As a result, as in Case 1 (see Fig. 12b), the magnitude of feedback is close to zero.

In conclusion, when using the existing map-based feed-forward controller, the control performance is not good because the magnitude of the feedback is mainly due to the significant error of the map-based feed-forward. However, the feedback gain can be reduced by using the proposed observer-based control. In addition, the proposed observer has the advantage of obtaining a near-optimal observer gain without a large amount of computation.

D. Comparison with Kalman filter

The proposed observer made additional comparisons with the two Kalman filters. First, the conventional Kalman filter used the states as $[\omega_t \ \omega_w \ T_o \ T_L]^T$. The model is constructed using (1), and assuming that the load torque's derivative is 0. Since it is necessary to estimate the load torque value, it has a disadvantage that T_{drag} cannot be estimated. In order to use the engine map for the Kalman filter, the DDO form should be used. The second Kalman filter (DDO) has the same form as Equations 5, 6, and 7, and only L_k is changed to Kalman gain. The Kalman filters have much computation because they have to compute 4×4 and 2×2 inverse matrices at every step, respectively.

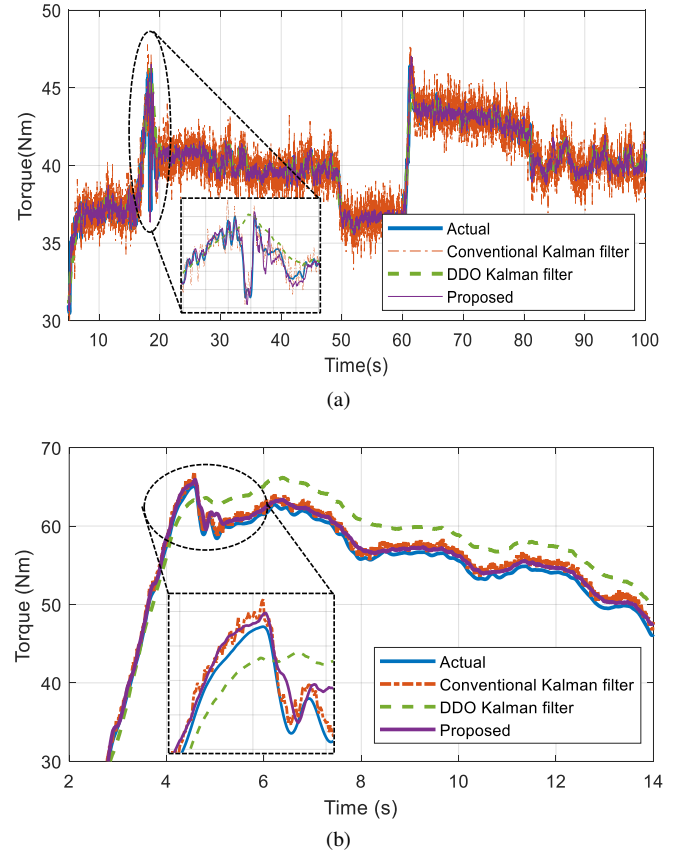


Fig. 13: Estimation result. (a) Case 1. (b) Case 2.

Through Fig. 13, it can be confirmed that the proposed observer shows superior performance with less computational

amount compared to the Kalman filter. Conventional Kalman filter uses only speed sensors. It is almost the same as reducing the map's dependence and increasing the model's dependence in the proposed method. Therefore, It shows almost the same performance with proposed method in a transient situation. However, since the engine map is not used in a steady state situation, it is more sensitive to noise. Since the DDO Kalman filter uses y_2 , it is not sensitive to noise, but it can be seen that an error occurs due to the error of y_2 in the transient part. This is because, Kalman gain calculates the optimal value in real-time, but it is not calculated considering the map used in y_2 has errors in the transient situation. The estimation errors of the observer are compared through NRMS(Normalized Root Mean Square), and the results are shown in Table I.

TABLE I: Estimation results (NRMS \times 100)

Road	Conventional Kalman	DDO Kalman	Proposed
Case 1	1.55	0.79	0.48
Case 2	1.43	5.67	1.37

VI. CONCLUSIONS

In this paper, an observer-based controller was proposed for a TC slip system. Due to the characteristics of the TC slip system, there are problems with uncertainty and an error from the steady-state map for model-based control. Therefore, in this paper, model-based control was carried out considering the error of the TC map and the engine map. The TC map was updated in real-time using RLSE, and the engine torque error was solved through the proposed observer. The proposed observer can change the pole to the desired position by adjusting the reliability of the sensor through the current characteristics of the system plant. It has been demonstrated that the error dynamics of the observer converge when only the initial tuning parameters are set according to the conditions, without complicated calculations. As a result, a near-optimal gain can be obtained based on the characteristics of the system without much computation.

The proposed observer was combined with DDO in this study to solve the noise sensitivity problem of the existing DDO. The slip-control performance was improved through accurate estimation while reducing the matrix size through DDO and reducing the amount of computation using the observer. The proposed method was verified through experimental data-based simulation. This control technique has the advantage of maximizing the feed-forward performance, unlike existing studies focusing on feedback control due to model inaccuracy and system uncertainty.

The proposed observer can be applied to any mechanical system that wants to change the reliability of the sensor over time. Therefore, depending on the method of setting the observer index, it is expected that it could be applied to various systems other than the TC.

It is worth pointing out that a proposed observer should be performed under linear systems. Therefore, the research should be extended to nonlinear systems. Also, we only prove the stability of the observer. Therefore, our future work will

be on how the observer index using fuzzy affects the observer performance. In addition, since fuel economy and ride comfort are determined by slip reference, an optimal slip reference generator should be studied.

REFERENCES

- [1] R. Hibino, M. Osawa, H. Yamada, K. Kono, and M. Tanaka, "H/sup/spl infin//control design for torque-converter-clutch slip system," in *Proceedings of 35th IEEE Conference on Decision and Control*, vol. 2. IEEE, 1996, pp. 1797–1802.
- [2] M. Osawa, R. Hibino, M. Yamada, K. Kobo, and Y. Kobiki, "Application of hinf control design to slip control system for torque converter clutch," *IFAC Proceedings Volumes*, vol. 28, no. 1, pp. 157–162, 1995.
- [3] H. Dourra, G. Kedar-Dongarkar, S. Elashhab, and M. Zohdy, "Torque converter clutch control using h ∞ loop shaping," SAE Technical Paper, Tech. Rep., 2009.
- [4] R. Hibino, M. Osawa, K. Kono, and K. Yoshizawa, "Robust and simplified design of slip control system for torque converter lock-up clutch," *Journal of dynamic systems, measurement, and control*, vol. 131, no. 1, 2009.
- [5] K. Hebbale, C. Lee, F. Samie, C.-K. Kao, X. Chen, J. Horgan, and S. Hearld, "Model based torque converter clutch slip control," SAE Technical Paper, Tech. Rep., 2011.
- [6] J.-O. Hahn and K.-I. Lee, "Nonlinear robust control of torque converter clutch slip system for passenger vehicles using advanced torque estimation algorithms," *Vehicle System Dynamics*, vol. 37, no. 3, pp. 175–192, 2002.
- [7] Y. Umemura and N. Sakamoto, "Optimal servo design for lock-up slip control for torque converter—nonlinear output regulation approach," *IEEE Transactions on Control Systems Technology*, vol. 23, no. 4, pp. 1587–1593, 2014.
- [8] B. Gao, H. Chen, and K. Sanada, "Clutch slip control of automatic transmission using backstepping technique," in *2009 ICCAS-SICE*. IEEE, 2009, pp. 3015–3019.
- [9] J. Oh, S. B. Choi, Y. Chang, and J. Eo, "Engine clutch torque estimation for parallel-type hybrid electric vehicles," *International Journal of Automotive Technology*, vol. 18, no. 1, pp. 125–135, 2017.
- [10] M. Diachuk and S. M. Easa, "Modeling combined operation of engine and torque converter for improved vehicle powertrain's complex control," *Vehicles*, vol. 4, no. 2, pp. 501–528, 2022.
- [11] A. J. Kotwicki, "Dynamic models for torque converter equipped vehicles," *SAE Transactions*, pp. 1595–1609, 1982.
- [12] D. Hrovat and W. Tobler, "Bond graph modeling and computer simulation of automotive torque converters," *Journal of the Franklin institute*, vol. 319, no. 1-2, pp. 93–114, 1985.
- [13] B. Pohl, "Transient torque converter performance, testing, simulation and reverse engineering," *SAE transactions*, pp. 201–216, 2003.
- [14] J.-H. Lee, "Control oriented modeling of dynamic torque converter system," in *2017 7th International Conference on Modeling, Simulation, and Applied Optimization (ICMSAO)*. IEEE, 2017, pp. 1–5.
- [15] K. Yi, B.-K. Shin, and K.-I. Lee, "Estimation of turbine torque of automatic transmissions using nonlinear observers," *J. Dyn. Sys., Meas., Control*, vol. 122, no. 2, pp. 276–283, 2000.
- [16] J.-O. Han, B.-G. Sin, H.-S. Jo, and G.-I. Lee, "Fuzzy logic slip control of torque converter clutch system for passenger car considering road grade resistance," *Transactions of the Korean Society of Mechanical Engineers A*, vol. 24, no. 3, pp. 718–727, 2000.
- [17] K. D. Mishra and K. Srinivasan, "On-line identification of a torque converter model," *IFAC-PapersOnLine*, vol. 50, no. 1, pp. 4763–4768, 2017.
- [18] J. Oh, J. Kim, and S. B. Choi, "Design of estimators for the output shaft torque of automated manual transmission systems," in *2013 IEEE 8th Conference on Industrial Electronics and Applications (ICIEA)*. IEEE, 2013, pp. 1370–1375.
- [19] X. Zhu and W. Li, "Takagi–sugeno fuzzy model based shaft torque estimation for integrated motor–transmission system," *ISA transactions*, vol. 93, pp. 14–22, 2019.
- [20] J. Park, S. Choi, J. Oh, and J. Eo, "Engine net torque compensation through driveline torque estimation in a parallel hybrid vehicle," *International Journal of Automotive Technology*, vol. 20, no. 3, pp. 619–627, 2019.
- [21] H. Choi, J. Hwang, and S. Choi, "Dynamic driveline torque estimation during whole gear shift for an automatic transmission," *Mechanism and Machine Theory*, vol. 130, pp. 363–381, 2018.

- [22] X. Yu, T. Shen, G. Li, and K. Hikiri, "Model-based drive shaft torque estimation and control of a hybrid electric vehicle in energy regeneration mode," in *2009 ICCAS-SICE*. IEEE, 2009, pp. 3543–3548.
- [23] X. Zhu, H. Zhang, B. Yang, and G. Zhang, "Cloud-based shaft torque estimation for electric vehicle equipped with integrated motor-transmission system," *Mechanical Systems and Signal Processing*, vol. 99, pp. 647–660, 2018.
- [24] J. Wu, P. D. Walker, J. Ruan, and N. Zhang, "Target torque estimation for gearshift in dual clutch transmission with uncertain parameters," *Applied Mathematical Modelling*, vol. 51, pp. 1–20, 2017.
- [25] Z. Zhao, L. He, Y. Yang, C. Wu, X. Li, and J. K. Hedrick, "Estimation of torque transmitted by clutch during shifting process for dry dual clutch transmission," *Mechanical Systems and Signal Processing*, vol. 75, pp. 413–433, 2016.
- [26] M. S. R. Mousavi, H. V. Alizadeh, and B. Boulet, "Estimation of synchronesh frictional torque and output torque in a clutchless automated manual transmission of a parallel hybrid electric vehicle," *IEEE Transactions on Vehicular Technology*, vol. 66, no. 7, pp. 5531–5539, 2016.
- [27] H. Trinh, T. D. Tran, and T. Fernando, "Disturbance decoupled observers for systems with unknown inputs," *IEEE Transactions on Automatic Control*, vol. 53, no. 10, pp. 2397–2402, 2008.
- [28] J. J. Oh, S. B. Choi, and J. Kim, "Driveline modeling and estimation of individual clutch torque during gear shifts for dual clutch transmission," *Mechatronics*, vol. 24, no. 5, pp. 449–463, 2014.
- [29] S. Kim and S. Choi, "Control-oriented modeling and torque estimations for vehicle driveline with dual-clutch transmission," *Mechanism and Machine Theory*, vol. 121, pp. 633–649, 2018.
- [30] D. Simon, *Optimal state estimation: Kalman, H infinity, and nonlinear approaches*. John Wiley & Sons, 2006.
- [31] M. Hou and P. Muller, "Disturbance decoupled observer design: A unified viewpoint," *IEEE Transactions on automatic control*, vol. 39, no. 6, pp. 1338–1341, 1994.
- [32] S. Boyd, V. Balakrishnan, E. Feron, and L. ElGhaoui, "Control system analysis and synthesis via linear matrix inequalities," in *1993 American Control Conference*. IEEE, 1993, pp. 2147–2154.
- [33] F. Cheli, E. Sabbioni, M. Pesce, and S. Melzi, "A methodology for vehicle sideslip angle identification: comparison with experimental data," *Vehicle System Dynamics*, vol. 45, no. 6, pp. 549–563, 2007.
- [34] J. Deur, J. Petric, J. Asgari, and D. Hrovat, "Modeling of wet clutch engagement including a thorough experimental validation," *SAE transactions*, pp. 1013–1028, 2005.
- [35] Y. Yang, R. C. Lam, and T. Fujii, "Prediction of torque response during the engagement of wet friction clutch," *SAE transactions*, pp. 1625–1635, 1998.
- [36] E. Berger, F. Sadeghi, and C. Krousgrill, "Analytical and numerical modeling of engagement of rough, permeable, grooved wet clutches," 1997.



Seibum B. Choi received the B.S. degree in mechanical engineering from Seoul National University, Seoul, South Korea, in 1985, the M.S. degree in mechanical engineering from the Korea Advanced Institute of Science and Technology (KAIST), Daejeon, South Korea, in 1987, and the Ph.D. degree in controls from the University of California, Berkeley, CA, USA, in 1993. From 1993 to 1997, he was with the Institute of Transportation Studies, University of California, working on the development of automated vehicle control systems. Through 2006, he was with TRW, Livonia, MI, USA, where he worked on the development of advanced vehicle control systems. Since 2006, he has been with the Faculty of the Mechanical Engineering Department, KAIST. His research interests include fuel-saving technology, vehicle dynamics and control, and active safety systems. He is a Member of the American Society of Mechanical Engineers, the Society of Automotive Engineers, and the Korean Society of Automotive Engineers.



Youngkwon Kim received the B.S. and M.S. degrees in mechanical engineering from Yonsei University, Seoul, Korea, in 1997 and 1999. Since 2002, he has been a research engineer with the HMC R&D division. His research interests include vehicle drivability, fuel/electric efficiency development with engine/transmission/power electric HW maTChing, and control tuning.



Byungjun Kim received his B.S. degree in Mechanical Engineering from Gwangju Institute of Science and Technology (GIST), Gwangju, Korea, in 2018 and M.S in Mechanical Engineering from the Korea Advanced Institute of Science and Technology (KAIST), Daejeon, Korea, in 2020, respectively. Since 2020, he is currently pursuing a Ph.D. degree in Mechanical engineering at KAIST. His research interests include powertrain system modeling and control, vehicle dynamics and control, and control theory.